Limit Analysis of a Soil Reinforced by Micropile Group: A Decomposition Approach

Z. Kammoun, J. Pastor, and H. Smaoui

Abstract The behavior of soils reinforced by micropile networks is still not fully understood due to the lack of accurate modelling capabilities. Particularly, the complex geometry of large soil-micropile systems makes accurate calculation of the bearing capacity of the reinforced soil a computational challenge. This complexity requires highly detailed and finely discretized models to achieve reasonable accuracy using direct numerical methods. Such models lead to large scale numerical optimization problems that are hardly tractable using a personal computer.

Recently a decomposition strategy with domain overlap has proved successful in solving very large kinematic and static limit analysis problems with limited computing resources. It consists of splitting the original problem into limit analysis subproblems that are smaller in size.

The present paper reports enhancements made to the original decomposition method. In particular, the method is made capable of solving the classical punch problem with Tresca or Coulomb soils. This benchmark problem is considered as a limit case of a soil reinforced by micropiles.

The paper then describes the application of the decomposition method to determine rigorous kinematic and static bounds to the bearing capacity of a soil reinforced by a micropile group according to a 2D plane strain model.

1 Introduction

A micropile is a pile with a diameter no greater than 250 mm, generally in the range 75 to 200 mm, usually with an aspect ratio of 200. Micropile technique was initially

Z. Kammoun (✉) · H. Smaoui
Ecole Nationale d'Ingénieurs de Tunis, LR11ES16 Laboratoire de Matériaux, Optimisation et Energie pour la Durabilité, Université de Tunis El Manar, 1002, Tunis, Tunisie
e-mail: kammounzied@yahoo.fr

H. Smaoui
e-mail: hichem.smaoui@enit.rnu.tn

J. Pastor
Laboratoire LOCIE, Polytech'Savoie, Université de Savoie, 73376 Le Bourget du Lac, France
e-mail: joseph.pastor@univ-savoie.fr

G. Saxcé et al. (eds.), *Limit State of Materials and Structures*,
DOI 10.1007/978-94-007-5425-6_10,

developed by the Fondedile company under the authority of F. Lizzi [5] as early as 1952. Micropiles were used for the first time in Italy in soil reinforcement of existing buildings and were then named root piles (*pali radice*). Within the timeframe of half a century, the technique has been applied all over the world [2].

The ease of their execution makes micropiles suitable for foundation works beneath existing buildings. Landmark examples are the Orsay railway station works for the development of a museum, "la Maladière" stadium in Neuchâtel in Switzerland (1100 micropiles) and the international airport of Boston (800 micropiles).

The complex geometry of large soil-micropile systems makes accurate calculation of the bearing capacity of the reinforced soil difficult because of the large size of the associated finite element model. As a strategy to handle problem sizes beyond available machine capacities, it is common to split the original problem into limit analysis (LA) subproblems that are smaller in size or simpler to solve.

In the present paper, the decomposition method, proposed in [7] and [8] in the framework of mixed kinematic limit analysis and extended in [3] and [4] to the static limit analysis problem, is adapted and applied to determine upper and lower bounds for the bearing capacity of micropile groups. The paper begins with a brief presentation of limit analysis followed by a description of the decomposition method. Next, the decomposition is applied to the punch problem (with Tresca or Coulomb soil), a representation of Prandtl's classical problem with finite domain. This benchmark example is considered here for (i) being a simple problem for which the solution is known a priori, (ii) being interpretable as a limit case of a soil reinforced by micropiles, that is the case with no reinforcement, (iii) exhibiting a feature that has not been tested so far in decomposition, that is the absence of a loaded zone in some subproblems.

Finally, the decomposition is exploited in the calculation of lower and upper bounds for the bearing capacity of examples of micropile groups.

2 Succinct Presentation of Limit Analysis

For the sake of clarity, without any loss in generality, we consider here that the velocity fields are continuous.

According to Salençon [9], a stress tensor field σ is said to be admissible if it is both statically admissible (SA, i.e., equilibrium equations, stress vector continuity, and stress boundary conditions are verified) and plastically admissible (PA, i.e., $f(\sigma) \leq 0$, where $f(\sigma)$ is the (convex) plasticity criterion of the material). Similarly, a strain rate tensor field v is admissible if it is kinematically admissible (KA, i.e., derived from a piecewise continuous velocity vector field u, with bounded discontinuities $[u]$, such that the velocity boundary conditions are verified) and plastically admissible (PA, i.e., the associated flow rules (2a), (2b) are verified).

A solution to the LA problem is a pair of fields (σ, v) where σ and v are both admissible and associated by the normality law. Classically, these solutions can be

found or approached using two methods. The first one, involving only the stresses as variables, is the statical (or lower bound) method. The second one, involving only the displacement velocities as variables, is the classical kinematic (or upper bound) method.

2.1 The Kinematic Method

Let us assume, as in [9], that the virtual power rate of the external loads P_{ext} can be written as the scalar product of a loading vector Q, whose components are called here loading parameters; and a generalized velocity vector $q = q(u)$, the components of which are called kinematic parameters. Following [1], let us consider a KA virtual velocity field u; the virtual power principle (VPP) states that the stress tensor fields σ, the stress vector field T (on the velocity discontinuity surfaces), and the vector Q are in equilibrium if, for any KA u, the following variational equation holds:

$$P_{\text{ext}} = Q \cdot q(u) = \int_V \sigma : v \, dV + \int_{S_d} T \cdot [u] \, dS. \tag{1}$$

In (1), V is the volume of the mechanical system, and S_d is the union of the velocity discontinuity surfaces. The results in terms of Q will be interpreted as a kinematic bound if, at the appropriate points of V, the variables verify the following conditions, where u is KA and q^d is a fixed value of $q(u)$:

$$v = \lambda \frac{\partial f}{\partial \sigma}, \quad \lambda f(\sigma) = 0, \ \lambda \geq 0, \ f(\sigma) \leq 0; \tag{2a}$$

$$[u] = \xi \frac{\partial f_{nt}}{\partial T}, \quad \xi f_{nt}(T) = 0, \ \xi \geq 0, \ f_{nt}(T) \leq 0; \tag{2b}$$

$$q(u) = q^d. \tag{2c}$$

The criterion $f_{nt}(T)$ results from the projection of the plasticity criterion $f(\sigma)$ on the Mohr plane, where n is the normal to the element of the velocity discontinuity surface and $T = (\sigma_{nn}, \sigma_{nt})$ is the stress vector on this element. More precisely, $f_{nt}(T)$ is the solution of the following system:

$$f(\sigma_{nn}, \sigma_{tt}, \sigma_{nt}) = 0; \qquad \frac{\partial f}{\partial \sigma_{tt}} = 0. \tag{3}$$

It is worth noting that, if (2a) and (2b) are verified, the quantities $\sigma : v$ and $T \cdot [u]$ become the *convex* unit dissipated powers $\pi_V(v)$ and $\pi_d([u])$ of LA, respectively, i.e.:

$$\pi_V(v) = \sigma : v; \qquad \pi_d\big([u]\big) = T \cdot [u]. \tag{4}$$

Fig. 1 The punch problem

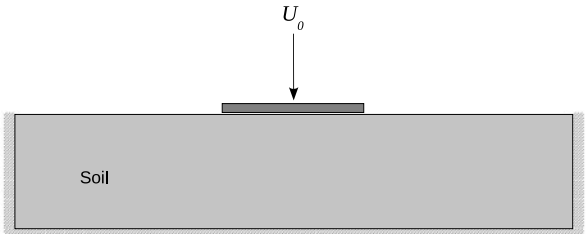

2.2 The Statical Method

The set of admissible loadings $Q = Q(\sigma)$, i.e. which are linearly associated with SA stress fields σ, forms a convex K in $\mathbb{R}^n$ and the n components of Q are called loading parameters.

Finding the solution of the static LA problem consists in finding an admissible field σ at the boundary ∂K of K by solving the following optimization problem

$$Q_{lim} = \left(Q_1^d, \ldots, \lambda_0 Q_i^d, \ldots, Q_n^d\right) \tag{5a}$$

$$\lambda_0 = \max\left\{\lambda,\, Q(\sigma) = \left(Q_1^d, \ldots, \lambda Q_i^d, \ldots, Q_n^d\right)\right\} \tag{5b}$$

where σ is an admissible stress field and Q^d a given admissible loading. This is the static, or lower bound method of LA that will be used here.

3 Decomposition of the LA Problem

3.1 The Kinematic Problem

For ease of presentation the decomposition of the kinematic problem is illustrated by applying it to the punch problem (Fig. 1).

A rigid plate, of width b supported by a soil, undergoes a downward motion with a uniform vertical velocity U_0 caused by a vertical force F applied at its center. Taking symmetry into account, only the left half of the plate, denoted V, is modeled. The domain V is meshed into 8×2 rectangles divided each into four triangles (Fig. 2). In the sequel, this mesh will be referred to as the target mesh (the mesh size will be defined by the number of its rectangular cells). The material of the soil is homogeneous, isotropic and is governed by the von Mises (or Tresca) criterion with cohesion c or by Coulomb's law with cohesion c and a friction angle φ. At the soil-plate interface, perfect bonding is assumed. This translates into kinematic boundary conditions in the soil given by prescribed vertical velocities equal to U_0 and zero tangential velocities. The static boundary conditions in the soil in contact with the plate are defined by unrestricted tangential stresses and by a normal stress resultant equal to the applied load F.

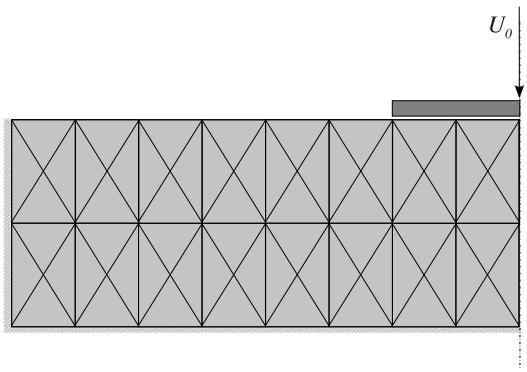

Fig. 2 Target mesh for domain V

The limit analysis problem associated with the load F applied to the soil domain V, discretized according to the target mesh, will be called the target problem and denoted P. It is defined by a unique loading parameter $Q = \frac{F}{bc}$ associated with the kinematic parameter $q^d = U_0$.

3.1.1 The Starting Problem

The decomposition procedure is initiated by solving a preliminary problem P_0, called the starting problem, which is small enough in size to be solvable using the available solution means. This problem is considered exclusively in the first iteration to provide an initial admissible velocity field for problem P.

A convenient choice for problem P_0 consists in replacing the target mesh by a coarser mesh made of a quarter (4×1) of the target number of rectangular cells, as shown in Fig. 3.

The solution of the starting problem provides an estimate of the velocities u^A and u^C at nodes A and C, respectively. The velocity u^B at B is deduced by linear interpolation. These three velocities are collected to form a vector U^{11} to be used in writing the boundary conditions for the subproblems in Step 2.

3.1.2 The Second Step

In Step 2 of the first iteration, the domain V is partitioned into 2 sub-domains, denoted V_{2i} $(i = 1, 2)$, bounded by the interface ABC (Fig. 3). To each subdomain V_{2i}, meshed into 4 cells, is associated an independent limit analysis subproblem denoted P_{2i}. The functional to be minimized in each of these subproblems is the power dissipated within the corresponding subdomain. The assembly of the optimal subproblem solutions gives an admissible solution for the target problem P over the complete domain V. Therefore, the sum of the subproblem powers can be set equal to FU_0. At this Step, the dissipated power is less than or equal to that of the starting problem. For the solution process to proceed from one iteration to another, the velocities (U^{11}) at the interface need to be updated. It should be noted that, in subsequent iterations, Step 2 will be repeated in the same way as presented above.

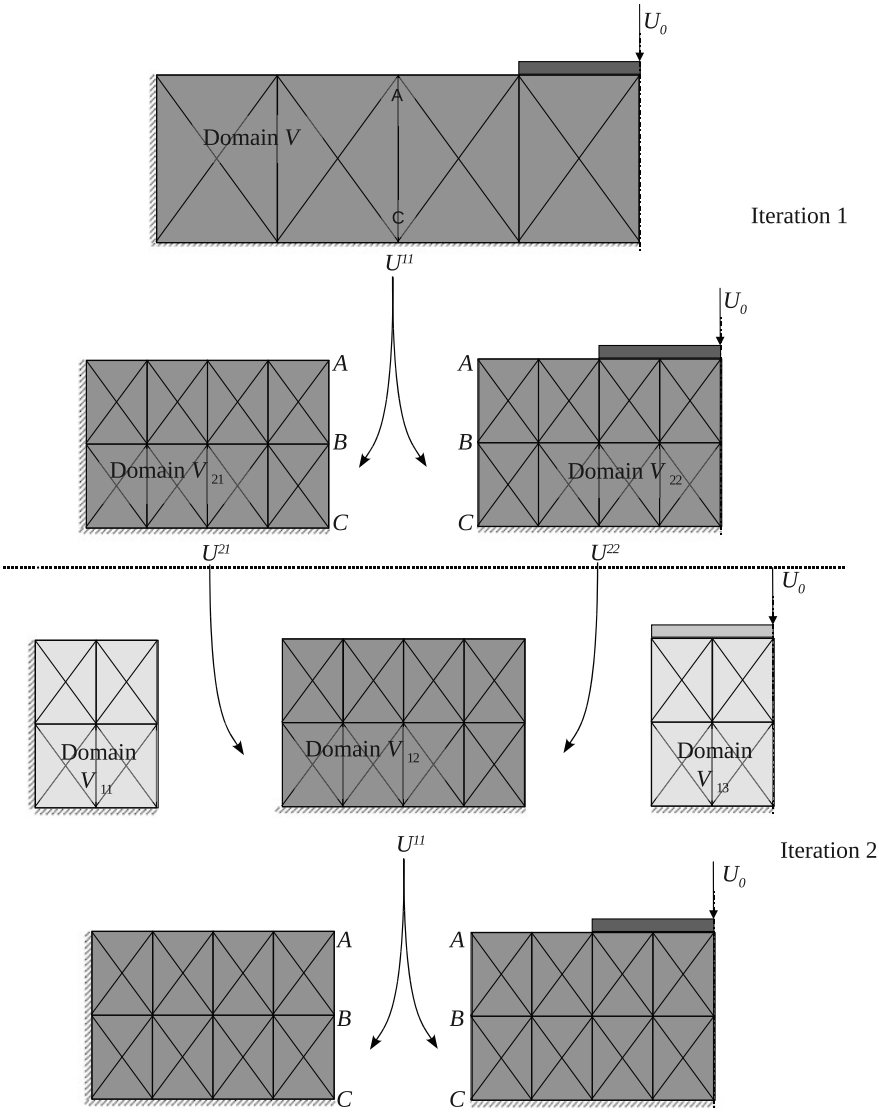

Fig. 3 Decomposition flow diagram

3.1.3 The Iterative Process

In subsequent iterations, the aim of the first step, labeled Step 1, is to improve the values of the velocities at the interface. For this purpose, the domain V is partitioned, without change in the discretization, into different sets of subdomains, denoted V_{1i} (Fig. 3), such that the interfaces between subdomains V_{2i} lie in the interior of subdomains V_{1i}. In an analogous way to Step 2, to each set V_{1i} is associated a LA

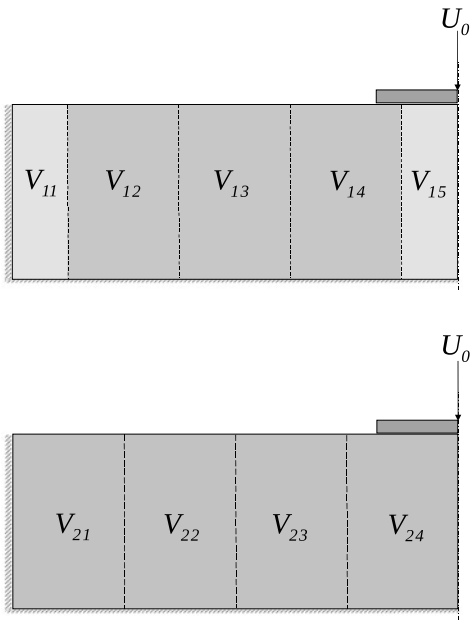

Fig. 4 The two partitions of the punch problem

subproblem P_{1i}. The velocities U^{2i} $(i = 1, 2)$ imposed at the interfaces are provided from the preceding step. The interface in Step 2 being in the interior of subdomain V_{12}, solving subproblem P_{12} allows the interface velocities to evolve. From the second iteration onward, all iterations are similar. The iterative process terminates when the progress in the solution from one iteration to another becomes small.

3.1.4 Partition into Many Subdomains

In general, the domain is partitioned into as many sub-domains as needed to bring the sub-problem down to a desired size. For instance, in the next section the decomposition is applied to the punch problem using a five sub-domain partition in Step 1 (Fig. 4).

For the first Step of the second and following iterations, solving only the three subproblems P_{12}, P_{13} and P_{14} is sufficient for updating the interface velocities previously blocked during Step 2.

3.2 Decomposition of the Static Problem

Using the punch problem again as an example, with a single loading parameter $Q = \frac{F}{bc}$ associated with the kinematic parameter $q^d = U_0$, the decomposition of the static problem proceeds in a manner basically similar to the decomposition of

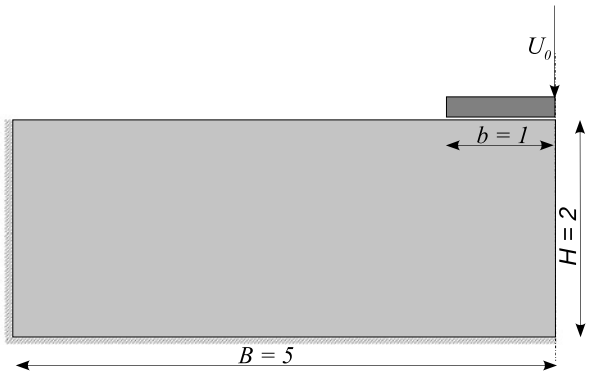

Fig. 5 Geometric data for the punch problem

the kinematic problem. In the first iteration, a starting problem P_0 is constructed. The domain V_0 associated to problem P_0 is discretized into four times fewer finite elements than the target problem domain V. As shown in Fig. 4, the domain V is partitioned alternatively into four sub-domains denoted V_{2i} or five sub-domains denoted V_{1i}. Solving problem P_0 constitutes the first step in this first iteration. The solution of problem P_0 provides a statically admissible first approximation of the stress field, including at the interfaces between sub-domains V_{2i}, as well as a lower bound for the limit load.

In the second step of the present iteration, stress components at the interfaces, obtained from the solution of problem P_0, are collected into so called interface stress vectors T_{1j}. The latter will serve in defining the boundary conditions for sub-problems (P_{2i}).

To cause changes in the stress field when solving these sub-problems, an alternative sub-problem formulation definition is proposed as follows. For each of sub-problems (P_{21}) to (P_{23}), the cohesion is treated as a variable parameter and solving problem P_{2i} consists in minimizing the corresponding cohesion subject to static admissibility constraints. This leads to solutions that are plastically admissible with maximal strength reserve. The solution of problem (P_{24}) provides the load resulting from the sub-problems of Step 1. The above process is repeated in the subsequent steps while alternating the domain partitions V_{1i} and V_{2i}.

4 Numerical Results for the Punch Problem

To assess the performance of the decomposition approach in solving the kinematic problem, the punch problem is solved using the data given in Fig. 5. For a Tresca soil with cohesion c the exact solution should be identical to that of a punch over a semi-infinite medium, known to be $F/(bc) = \pi + 2$. This is because Prandtl's mechanism, which corresponds to the exact solution of the semi-infinite soil, can be fitted in the selected volume. This allows comparison of results to a known exact solution.

Table 1 Kinematic bound $\frac{F}{bc}$ for the punch problem with a Tresca soil

Mesh	Number of elements	Direct			Decomp. (1 iter.)		
		$F/(bc)$	Accuracy	CPU(s)	$F/(bc)$	Accuracy	CPU(s)
40×18	2880	5.1787	3.5×10^{-7}	578	5.2681	3.6×10^{-7}	15
80×36	11520	5.1607	4.4×10^{-7}	3595	5.1629	4.6×10^{-7}	1985
160×72	46080	5.1519	7.1×10^{-7}	38211	5.1526	5.5×10^{-7}	21912
320×144	184320	—	—	—	5.1476	3.8×10^{-7}	184550

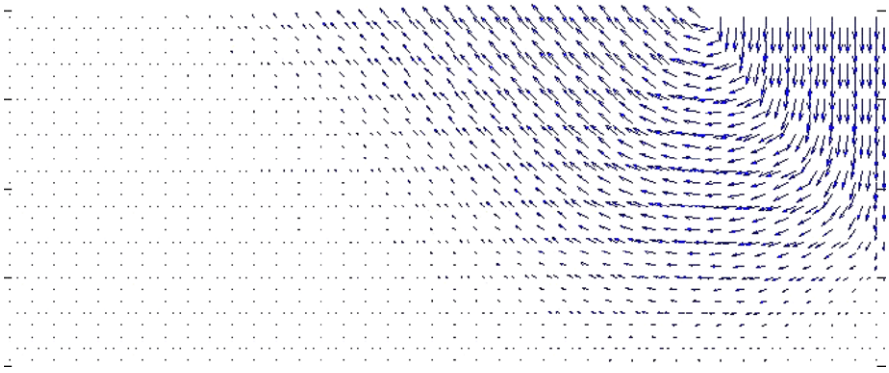

Fig. 6 Velocity field in the punched soil. First iteration of the decomposition

4.1 Kinematic Solution

Upper bounds for the punch problem are determined based on different levels of discretization and using both the direct approach and a single iteration of the decomposition method for solving the kinematic problem. The decomposition is applied based on the domain partitions shown in Fig. 4.

The numerical optimization problems arising from the limit analysis (sub)problems involved in the present example, as well as all subsequent examples treated in this paper, are all solved using the conic programming code MOSEK [6] and run on a Mac Pro 3 GHz machine with 12 Gb of RAM.

Table 1 shows the upper bounds obtained for the punch problem based on various discretizations. In a first series of runs the soil is characterized by a Tresca criterion with cohesion $c = 1$. For large mesh size (184 320 elements), the problem can only be solved using decomposition, giving the upper bound 5.1476 and a relative error of 0.12 % with respect to the exact solution.

The velocity field resulting from the first iteration is visualized in Fig. 6 for an 80×36 mesh (Tresca, $c = 1$). The failure mechanism can be clearly seen, with the velocities gradually decreasing downward until they vanish at the substrate. Considering a soil governed by a Coulomb criterion with the same cohesion $c = 1$ and a friction angle φ, the upper bound is determined for various friction angles, based on

Table 2 Kinematic bound $\frac{F}{bc}$ for the punch problem (Coulomb soil, 11520 elements)

φ (°)	Decomp. it1	Direct	Relative err.
0	5.1628	5.1607	0.04 %
5	6.5075	6.5062	0.02 %
10	8.3773	8.3752	0.03 %
15	11.0497	11.043	0.06 %
20	15.1819	15.1621	0.13 %
25	22.3637	22.3236	0.18 %
30	36.6335	36.5231	0.30 %

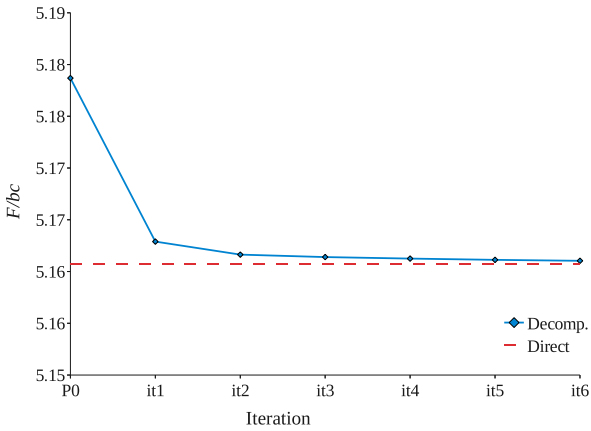

Fig. 7 Decomposition iteration history

an 80 × 36 mesh (11 520 finite elements). Table 2 shows the upper bounds obtained using direct problem solution and using a single iteration of the decomposition for different values of the friction angle. The relative error of the decomposition result with respect to the direct solution is less than 0.3 %.

The iteration history displayed in Fig. 7 for the Tresca soil shows that a few iterations are needed to converge to the target value known from the direct solution.

4.2 Static Solution

The static problem is solved to determine lower bounds for the punch problem with a Tresca soil. Different mesh sizes are considered. Calculations are carried out by solving the problem both directly and using one iteration of the decomposition method based on the same domain partitions as in the kinematic case (Fig. 4). All (sub)problems are solved using the MOSEK code run on the Mac Pro 3 GHz machine.

Post analysis verification of constraint violation shows that accuracy of the solution varies from 10^{-9} for a 1600 element to 10^{-5} for a 102400 element mesh. With

Table 3 Static bound F/bc for punch problem (Tresca soil)

Mesh	Number of elem.	Decomp. it1	Direct	Error/direct	Error/theoretical
40×10	1600	5.0989	5.1094	0.21 %	0.83 %
80×20	6400	5.1185	5.1236	0.1 %	0.45 %
160×40	25600	5.1277	5.1329	0.1 %	0.27 %
360×80	102400	5.1358	5.1372	0.03 %	0.11 %
720×160	409600	5.1387	—	—	0.06 %

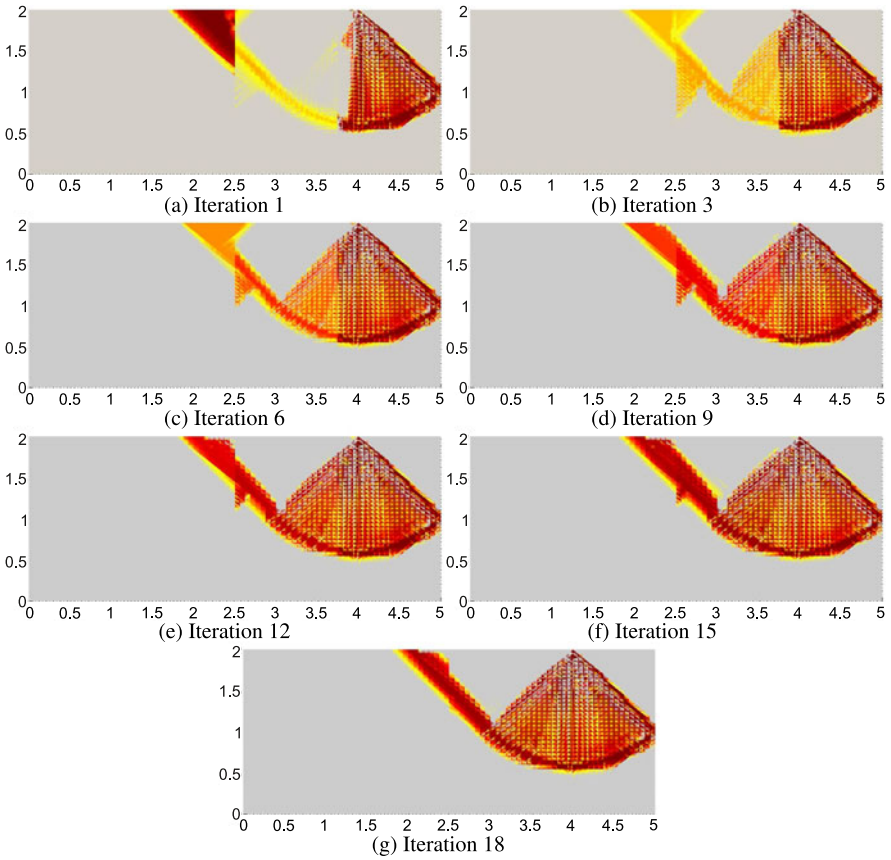

Fig. 8 Visualization of failure zones in the soil

a 409600 element discretization, the direct solution appears to be impossible using the same machine with 12 Gb of RAM.

For this run, the decomposition result is within 0.06 % of the theoretical solution (Table 3). For the 80×40 mesh, the decomposition is exceptionally carried out up to the 18th iteration and the evolution of the failure zone throughout the iterations

Table 4 Static bounds ($F/(b\,c)$) for the punch problem (Tresca and Coulomb)

φ (°)	Initial	Decomp. it1	Direct
0	5.125	5.128	5.133
5	6.462	6.467	6.468
10	8.304	8.308	8.316
15	10.910	10.920	10.928
20	14.884	14.903	14.934
25	21.710	21.759	21.867
30	34.920	35.094	35.402

is visualized in Figs. 8 ((a)–(g)). These figures show the zones where the failure criterion lies in the narrow range -0.005 to 0. A Prandtl like mechanism is clearly exhibited as early as the first iteration except in the neighborhood of the interface. The disturbance in the stress field near the interface is seen to gradually diminish and eventually vanish. Next, a Coulomb soil is considered and a series of problems are solved with the same 80×40 mesh and different values of friction angle. Table 4 displays the static bounds for the Tresca and Coulomb criteria with cohesion $c = 1$ and friction angle φ varying from 5 to 30.

It is noted that, as observed with the Tresca criterion, a large improvement in the bound is achieved at the first iteration for all the tested friction angles.

The iteration history of the lower bound is plotted in Fig. 9 for the Tresca soil based on an 80×40 mesh. It shows that a few iterations only are needed to closely approach the target solution.

5 Bearing Capacity of Micropile Groups

5.1 Problem Description

The problem addressed in this work is that of a soil, bounded below by a substrate at depth H, to be reinforced by a group of micropiles, as shown in Fig. 10, with the purpose of supporting a load F. In the two dimensional representation adopted here the problem is interpreted as a plane strain one.

The numerical limit analysis (sub)problems are all solved using the same MOSEK code and Mac Pro machine as in the punch problem example.

5.2 Soil Reinforced with 9 Micropiles

Let us consider the following example of a soil reinforced with 9 micropiles. The soil is characterized by a Coulomb criterion with a cohesion of 10 kPa and friction

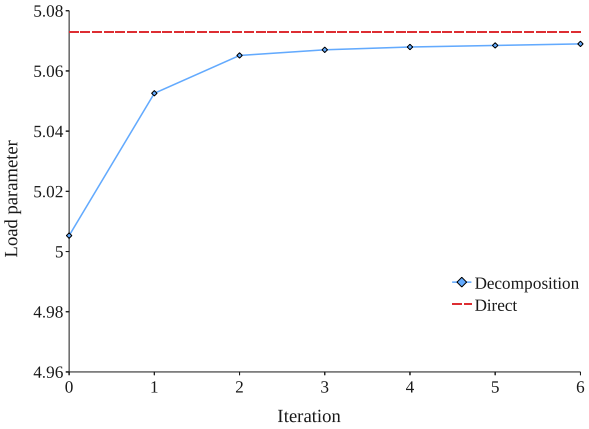

Fig. 9 Iteration history for the Tresca criterion

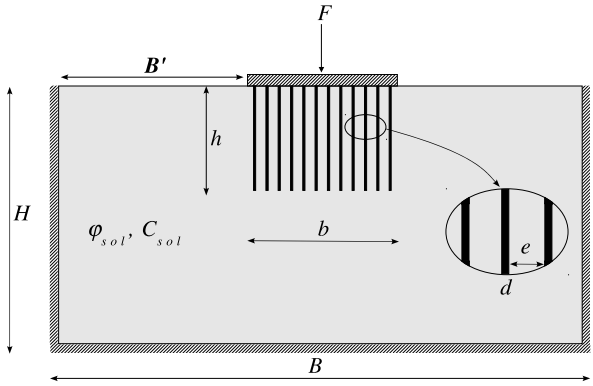

Fig. 10 Soil reinforced by a micropile group

Table 5 Geometric data of the reinforced soil (in meters)

H	h	B	d	Number of micropiles
10	5	24	0.1	9

angle $\varphi = 10°$. It is reinforced with micropiles characterized by a Tresca material with a cohesion of 10 MPa.

The geometry of the problem is summarized in Table 5.

It should be noted that the total load applied to the base is equal to F. Since the problem is symmetric, only half of the domain is modeled and the load to be maximized is reduced to $\frac{F}{2}$.

Table 6 shows the solutions obtained for different spacings between micropiles (e in Fig. 10) using the direct approach and the decomposition limited to the first iteration.

For meshes composed of more than 80.000 triangles for the static approach and 20.000 triangles for the kinematic approach, the MOSEK code fails to give fully optimal and admissible post-analyzed solutions. Beyond this limit, decomposition

Table 6 Soil reinforced with 9 micropiles

Spacing (m)			Mesh	$\frac{F}{2}$ (kN)	Accuracy	CPU (s)	Relative gap (%)
0.9	direct	static	480×30	482.21	1.6×10^{-7}	106	39.69
		kinem.	480×10	673.58	0.004	188	
	decomp.	static	960×60	486.23	3.4×10^{-5}	780	16.33
		kinem.	480×40	565.64	7.2×10^{-5}	2227	
0.7	direct	static	480×30	398.75	8.8×10^{-8}	119	49.02
		kinem.	480×10	594.20	7.9×10^{-5}	203	
	decomp.	static	960×60	403.27	1.6×10^{-4}	1043	20.46
		kinem.	480×40	485.79	9.3×10^{-4}	2637	
0.5	direct	static	480×30	322.39	5.4×10^{-8}	131	41.34
		kinem.	480×10	455.68	9.2×10^{-4}	207	
	decomp.	static	960×60	325.56	4.5×10^{-5}	980	16.98
		kinem.	480×40	380.84	5.2×10^{-5}	1672	
0.3	direct	static	480×30	247.13	1.8×10^{-8}	99	31.17
		kinem.	480×10	324.15	7.1×10^{-6}	99	
	decomp.	static	960×60	249.32	3.4×10^{-5}	757	11.51
		kinem.	480×40	278.01	2.7×10^{-5}	1474	

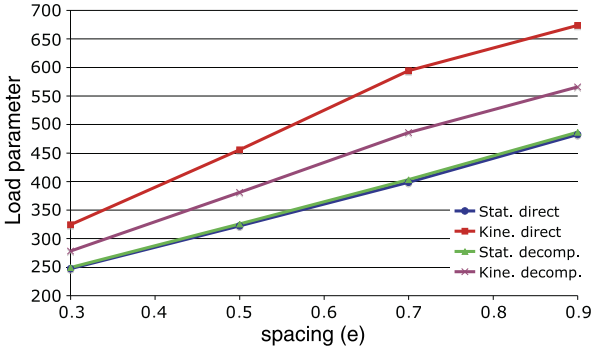

Fig. 11 Bounds for direct approach and decomposition

using 4-sub-domain partitions still converges using up to 300.000 triangles for the static approach and 80.000 triangles for the kinematic approach.

Decomposition has made possible a reduction by half of the gap between the upper and the lower bounds relative to the static bound with some improvement in the quality of the kinematic solution.

Figure 11 shows that the gap between static and kinematic bounds increases with spacing between micropiles.

Visualization of the failure zone (failure criterion) shows that the failure mechanism varies with spacing. For small spacing (Fig. 13), the failure zone in the soil

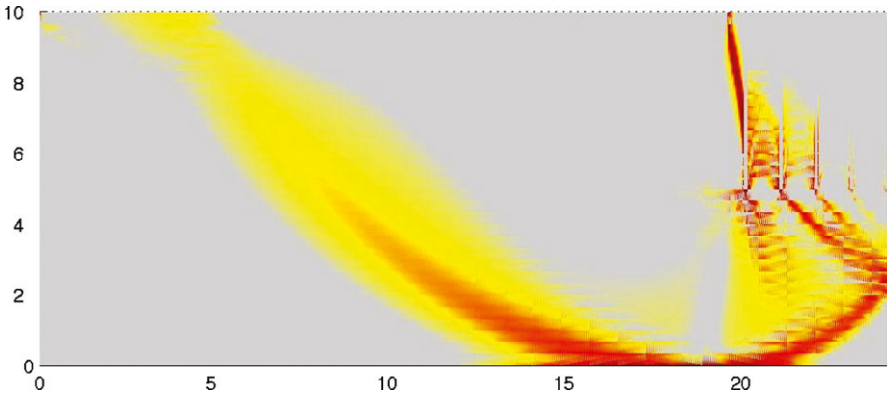

Fig. 12 Failure zone for 0.9 m spacing

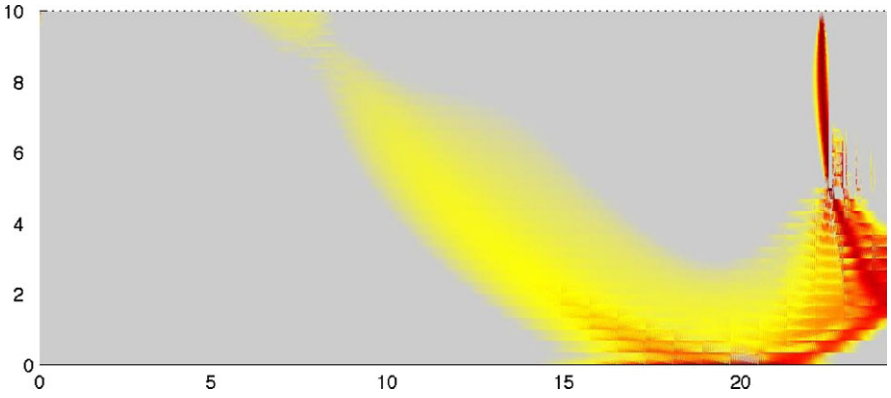

Fig. 13 Failure zone for 0.3 m spacing

is limited to the lower third of the reinforced zone, whereas for a 0.9 m spacing (Fig. 12), the failure zone covers two thirds of the depth of the reinforced zone.

5.3 Soil Reinforced by 17 Micropiles

In this example a Tresca soil with cohesion $c = 10$ kPa is reinforced with 17 micropiles made out of a Tresca material with cohesion $c = 5000$ kPa. The geometric data of the problem are given in Table 7.

Consider target problems modeled with an 800×16 mesh for the static approach and an 800×24 mesh for the kinematic approach. The solutions of all subproblems of the first iteration of the decomposition algorithm are reported in Table 8. In the static problem, the sub-problems (P_{21}), (P_{22}) and (P_{23}) need not be treated if the process is to be terminated at the first iteration. Their actual involvement in the

Table 7 Geometric data for a soil reinforced with 17 micropiles

H	h	B	d	e
20	15	80	0.2	0.8

Table 8 Bounds for bearing capacity of soil reinforced with 17 micropiles (Coarse discretization)

Sub-probl.	$Q = \frac{F}{2}$ (kN)		Accuracy		CPU (s)	
	Stat.	kinem.	Stat.	kinem.	Stat.	kinem.
0	736.2	1142.8	1.0×10^{-6}	2.3×10^{-5}	23	1169
11	–	1.6	4.7×10^{-7}	2.2×10^{-6}	49	1533
12	–	82.2	4.3×10^{-7}	5.7×10^{-6}	48	148
13	–	290.3	9.1×10^{-6}	6.7×10^{-6}	33	1878
14	781.7	709.6	6.1×10^{-5}	6.1×10^{-5}	32	1909
1^{st} it.	781.7	1083.8	6.1×10^{-5}	6.1×10^{-5}	183	6636

process begins at the second iteration because the associated sub-domains are not directly subjected to the applied load.

Conducting a single iteration of the decomposition algorithm, the relative difference between upper and lower bounds decreases from 55.23 % to 38.64 %.

Further improvement in the upper and lower bounds requires finer discretization, which leads to problem size that cannot be handled using the same domain partitions. A decomposition into smaller sub-domains would be needed to solve such a large problem. Using a finer partition, say with 9 (resp. 8) subdomains in Step 1 (resp. Step 2), the decomposition can be carried out at a single level, similarly to the example with 5 (resp. 4) subdomains. An alternative strategy is a multilevel scheme where each subproblem at one level of the decomposition is solved recursively by another level decomposition.

6 Conclusion

Rational sizing of soil reinforcement by micropile groups requires proper modeling of the soil-micropile system. Numerical methods for limit analysis are suitable for handling the geometric and behavioral complexities of the soil-micropiles system, however, they give rise to large size numerical nonlinear optimization problems. In the presented work, the decomposition approach has been adapted to the case of a Coulomb soil. Furthermore, for a Tresca as well as a Coulomb soil, the decomposition made it possible to solve larger problems than the direct method would allow, using the same machine. This led to an improvement of the lower and upper bounds for the bearing capacity of a soil reinforced by micropile groups. The gap between upper and lower bounds has been reduced by half compared to the best possible direct solution. The success of the decomposition method paves the way

to the treatment of the three dimensional problem which allows a far more realistic representation of the real soil-micropile system.

References

1. Anderheggen, E., Knopfel, H.: Finite element limit analysis using linear programming. Int. J. Solids Struct. **8**, 1413–1431 (1972)
2. Estephan, R.: Contribution aux méthodes de calcul des groupes et des réseaux de micropieux. Thèse de doctorat, ENPC, CERMES, Marne la Vallée (2003)
3. Kammoun, Z.: Prévision de la charge limite des sols renforcés par réseaux de micropieux. Thèse de doctorat, Université de Savoie et Ecole Nationale d'Ingénieurs de Tunis (2010)
4. Kammoun, Z., Pastor, F., Smaoui, H., Pastor, J.: Large static problem in numerical limit analysis: A decomposition approach. Int. J. Numer. Anal. Methods Geomech. (2010). doi:10.1002/nag.887
5. Lizzi, F.: The 'pali radice' (root piles)—a state of the art report. In: Symposium on Recent Developments in Ground Improvement Techniques, Bangkok, Thailand (1982)
6. MOSEK ApS: C/O Symbion Science Park, Fruebjergvej 3. Box 16, 2100 Copenhagen ϕ, Denmark (2002)
7. Pastor, F.: Résolution par des méthodes de point intérieur de problèmes de programmation convexe posés par l'analyse limite. Thèse de Doctorat, Facultés Universitaires Notre-Dame de la Paix Namur (2007)
8. Pastor, F., Loute, E., Pastor, J.: Limit analysis and convex programming: A decomposition approach of the kinematic mixed method. Int. J. Numer. Methods Eng. **78**, 254–274 (2009)
9. Salençon, J.: Théorie de la Plasticité Pour les Applications à la Mécanique des Sols. Eyrolles, Paris (1974)